Solid State Communications Journal Details

Detail	Information
Title	Solid State Communications
Publisher	Elsevier
Scope	The journal focuses on solid-state physics, including electronic properties of solids, superconductivity, magnetism, and optical properties of solids.
Frequency	Monthly
Website	https://www.journals.elsevier.com/solid-state-communications
Print ISSN	0038-1098
Electronic ISSN	1879-2766
Impact Factor	2.068 (as of 2022 Journal Citation Reports)
Ranking	Moderate impact within the field of solid-state physics journals
Peer Review Process	Peer-reviewed
Open Access Policy	Traditional subscription-based model (not open access)
Article Types	Research Articles, Review Articles, Short Communications
Editor-in-Chief	Specific names of the current editor-in-chief may vary; check the journal's website for updated information
Submission Process	Manuscripts can be submitted online via Elsevier's submission system
Publication Process	Accepted articles are published online and in print
Citation and Metrics	Citations can be tracked through databases like Scopus, Google Scholar, and Web of Science
Ethics Statement	Adheres to Elsevier's ethical guidelines, including conflicts of interest, ethical approval for human/animal research, and research integrity

Priyanka N. Thorat

Solid State Communications 390 (2024) 115599

Contents lists available at ScienceDirect

Solid State Communications

journal homepage: www.elsevier.com/locate/ssc

An Extensive analysis of the Janus Si_2XY (X, Y=P, As, Sb, Bi): Optical and biaxial strain dependent electronic properties

Priyankaben N. Thorat [a], Aparnakumari M. Patel [a], Rahulkumar P. Jadav [a], Radha N Somaiya [b,*], Yogesh Sonvane [a,**]

[a] Advanced Materials Lab, Department of Physics, Sardar Vallabhbhai National Institute of Technology, Surat, 395007, India
[b] Department of Physics, Indian Institute of Technology, Bombay, Mumbai, 400076, India

ARTICLE INFO

Communicated by: Ogut Gulseren

ABSTRACT

In the 2D materials field, Si_2XY Janus monolayers have gained more attention with the help of their distinct optical and electronic properties. The Ab Initio Molecular Dynamics (AIMD) method of the Si_2XY monolayers is found to be stable at ambient temperature. The electronic properties are helpful to find indirect bandgap characteristics in these monolayers, except for Si_2PBi. The effect of biaxial strain, the band engineering is studied. At higher strain values, bandgaps first rise to 1.34 eV, then fall to 0.72 eV, becoming conductive and after implementing the HSE06 functional, the pristine Si_2PAs system exhibited a higher band gap of 2.009 eV. Moreover, we explored the optical properties of Si_2XY Janus monolayers via calculations of the optical spectra, absorption, and refractive index, which indicated potential in the visible and infrared (IR) regions. Based on these results, a thorough understanding of Si_2XY Janus monolayers is offered via a change in material electronic nature via strain engineering and via optical properties, thus shows the area of optoelectronics application.

1. Introduction

Two-dimensional (2D) materials are gaining a lot of attention due to their distinctive optoelectronic properties ever since the experiment in 2004 that successfully polished graphene [1]. Newly developed 2D materials with uncommon electronic and optical characteristics include graphene [2,3], silicone [4–6] phosphorene [7,8], boron-nitride nanosheets [9–11], antimonene [12,13], and the monolayers of transition metal dichalcogenides (TMDCs) have superior electronic and optical characteristics [14–20]. These 2D materials are used to create the next-generation electronic devices and are unlike graphene in that they are classified as semiconductors.

Now a days, the 2D Janus materials are more beneficial due to their unique electronic characteristics and structures. Group IV-V material monolayers with A_2B_2-monolayer structures and unique electronic characteristics had been developed [21–24]. Huang et al. evaluated the solid-state chemistry of Si_xP_y ($1 \leq y/x$) utilizing a structure analysis method and found that the Si_2P_2 type monolayer (p6m2 space group) is also dynamically stable [25]. X_2Y_2 type IV-V monolayers (X = C, Si, Ge, Sn, Pb; Y=N, P, As, Sb, Bi) were studied for theoretical stability and electronic properties [26,27].

Previous evidence indicates that these system's first absorption peaks alongside within-plane polarization is located in the visible spectrum range [28]. Due to their higher absorption coefficient of visible spectra, these 2D materials are potential for use in electronic devices. These system structure could be generated from monochalcogenide and dichalcogenide monolayers [29]. The Janus and TMDC monolayers have been developed using the chemical vapor deposition (CVD) technique [30–33]. Group IV-V 2D binary monolayers like GeAs, GeP, SiAs, and SiP have piqued the curiosity of researchers from theoretical and experimentalstandpoints [34,35]. In modern day electronic devices, bandgap tunability of a semiconductor material is vital, which in particular, when the strain goes into effect, leads to a semiconductor-metal phase transition [36].

The asymmetric crystal structure offered via 2D Janus materials in comparison with conventional 2D materials. Tosuki et al. carried additional studies on the Rashba and electronic characteristics of Janus Si_2AB (A, B=P, As, Sb, and Bi) monolayers [37]. They showed that the strength of spin splitting in Rashba effect can be enhanced by applying stress. These diverse investigations underscore the significant

* Corresponding author.
** Corresponding author.
E-mail addresses: somaiyaradha@gmail.com (R.N. Somaiya), yas@phy.svnit.ac.in (Y. Sonvane).

https://doi.org/10.1016/j.ssc.2024.115599
Received 20 January 2024; Received in revised form 8 June 2024; Accepted 20 June 2024
Available online 21 June 2024

advantages offered by these 2D Janus systems in the field of electronics. Other Janus materials, including monolayers of Ge_2PAs, Si_2PAs, and Sn_2PAs, also hold promise [38,39]. Recent discoveries have revealed favorable piezoelectric properties and robust thermal stability in these materials, offering potential benefits in multifunctional sensing applications. Additionally, Vu et al. demonstrated that optical characteristics of Janus monolayer Ga_2SeTe can be significantly enhanced under strain [40]. After applying a strain, the Al_2SSe Janus monolayer's optical and electrical properties were also modified [41]. But until now, the Si_2XY monolayer's optoelectronic properties have not been systematically investigated. The study of the influence of strain on the bandgaps of the Janus Si_2XY monolayers are very significant for a basic theoretical based study of these monolayers. It follows that there is a clear reason to look into the optical properties of monolayer Janus Si_2XY (X, Y=P, As, Sb, and Bi) and its potential for use across numerous electronic device applications.

In this study, we conduct a comprehensive analysis of the crystal structure, electronic properties, strain effects, and optical characteristics of Janus Si_2XY (X, Y=P, As, Sb, Bi) monolayers. Additionally, we investigate the structural stability at ambient temperature using the NVT ensemble with an ab initio molecular dynamics (AIMD) approach. The analyzed properties include electronic density of states (DOS), band structure, optical absorption spectra, effects of biaxial strain on the bandgap, and molecular dynamics behavior. Our calculations reveal that employing the HSE06 parameter results in an expanded bandgap compared to the PBE parameter for all systems studied. Furthermore, biaxial strain is found to enhance the electronic properties of Janus Si_2XY monolayers and enables tuning of the bandgap. With a flexible bandgap ranging from 0.896 eV to 1.291 eV, these monolayers exhibit enhanced optical absorption in the visible spectrum, suggesting their potential suitability for optoelectronic devices.

2. Computational methodology

Here, the First Principles analysis to analyze the various characteristics of systems using the Projector-Augmented Wave (PAW) approach, which was employed in the Vienna Ab initio Simulation Package (VASP), and via the First Principles Approach [42–44]. When evaluating the various characteristics of 2D Janus Si_2XY monolayers, we implemented the generalized gradient approximation (GGA) that is provided by Perdew-Burke-Ernzerhof (PBE) functional and as well as hybrid HSE06 spanning exchange-correlation potential [45–47]. the energy and force parameters of 10^{-6} eV and 10^{-3} eV/Å are used to optimize the monolayer, respectively. The 20 Å vacuum zone is used to inhibit interactions in the conventional direction (Z-axis). For AIMD simulation the NVT ensemble with Andersen thermostat is used with 5 × 5 × 1 supercell of all systems at ambient temperature using time 5 ps and 1 fs timestep [48,49]. We used a larger (15 × 15 × 1) k-point mesh to achieve a significant outcome for the electrical properties. Here, a visualization tool called Vesta is employed to visualized relax structure [50].

3. Results and discussions

3.1. Structural properties

In this study, we performed structural analyses of 2D Si_2XY Janus monolayers, as illustrated in Fig. 1. The covalent bonding between two Si atoms and group-V atoms is evident in the side view, as depicted in Fig. 1(b). The hexagonal lattice structure is apparent from the top view, where each group-V atom forms bonds with three Si atoms. Structural parameters, band gap, and cohesive energy of this compound were computed and are presented in Table 1. Notably, unlike compounds containing N atoms (Si_2NY; Y=P, As, Sb, Bi), which exhibit instability and fail to satisfy the conditions for Born stability, the Si_2XY monolayers demonstrate stability. These investigations demonstrate an increase in the band gap value when employing the HSE06 method, as compared to previous studies conducted on Si_2XY systems [51]. The table presents the lattice constant values for stable structures, revealing that the lattice constant is smallest for the Si_2PAs monolayer and increases proportionally with the atomic radius. Si_2XY monolayers exhibit lattice constants that fall within the range observed for SiX and SiY compounds [52]. In this case, the lattice constants for SiP and SiAs fall within the range of 3.521–3.552 Å and 3.68 to 3.701 Å, respectively. The similar classes of CP, CAs, CSb, and CBi have a similar hexagonal structure with a lattice constant range from 2.901 to 3.601 Å [53]. The calculated lattice constant for Si_2PAs is 3.610 Å, which lies between the lattice constants of SiAs and SiP monolayers. To assess the stability of the 2D Si_2XY monolayer, the cohesive energy is determined using equation.

$$E_{coh} = \frac{2E_{Si} + E_P + E_{As} - E_{Si_2PAs}}{4} \quad (1)$$

$$E_f = \frac{E_{Si_2XY} - E_X - E_Y - 2E_{Si}}{n} \quad (2)$$

Here (eq. (1)), the letters E_{Si}, E_P, and E_{As} stand for the energies of Si, P, and As, as well as E_{Si_2PAs} indicates total energy of the system per unit cell. The Si_2PAs monolayer delivers the highest value of cohesive energy. It implies that the Si, P, and As atoms have a strong bonding. Cohesive energy values play a crucial role in assessing the stability of a system and provide insights into whether a process is exothermic or endothermic, as indicated by negative and positive cohesive energy values, respectively [54]. The Si_2PAs are more dynamically stable than other compounds in groups IV and V. Compared to SiX (X = N, P, As, Sb, Bi) system series

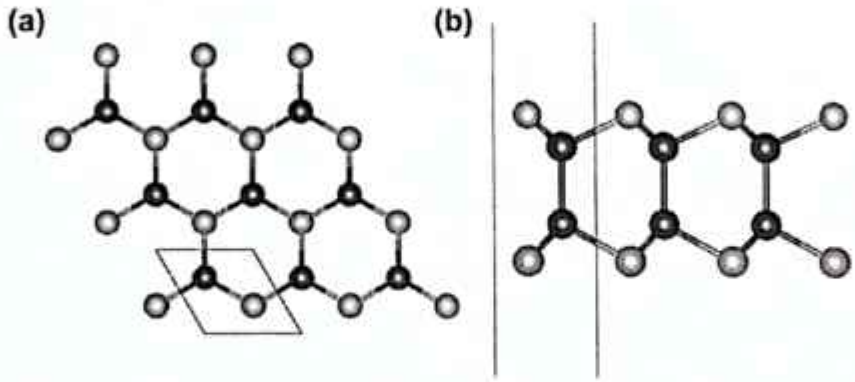

Fig. 1. Si_2XY monolayers are displayed in (a) top and (b) side view points, the colors of the Si, X, and Y atoms are blue, grey, and green. (For interpretation of the references to color in this figure legend, the reader is referred to the Web version of this article.)

Table 1
the lattice parameter (a), which defines what separation spaced Si, X, and Y atoms are in a primitive cell, bandgap E_g (PBE), cohesive energy E_c, formation energy E_f and work function φ of respective systems

System	a (Å)	d_{Si-X} (Å)	d_{Si-Y} (Å)	d_{X-Y} (Å)	d_{Si-Si} (Å)	E_g (eV)	E_c (eV/atom)	E_f (eV/atom)	φ (eV)
Si_2PAs	3.636	2.371	2.311	2.371	4.493	1.291	5.151	−0.317	5.329
Si_2PSb	3.759	2.362	2.362	2.553	4.631	0.237	4.829	−0.230	4.757
Si_2PBi	3.812	2.351	2.301	2.641	4.712	0	4.652	0.042	4.756
Si_2AsSb	3.853	2.363	2.463	2.572	4.711	0.827	4.663	−0.132	4.134
Si_2AsBi	3.919	2.352	2.498	2.650	4.791	0.149	4.511	−0.169	4.218
Si_2SbBi	4.008	2.351	2.651	2.701	4.870	0.896	4.340	−0.112	4.534

have cohesive energy in range of 3.5 eV/atom to 5.5 eV/atom with Si_2XY gives similar stable range [54]. The estimated cohesive energies are lower compared to 7.85 eV/atom of graphene and higher compared to graphene like g-SiC and SnBi (2.81 eV/atom) has similar structure like SiB [56–58]. From eq. (2), the E_f is formation energy of Si_2XY system, E_{Si_2XY} is energy of pristine Si_2XY system, n is number of atoms in systems, E_{Si}, E_X and E_Y are energy per atom of Si, X and Y atom in bulk form, respectively. According to the established definition, a negative formation energy indicates that the system is dynamically stable, while a positive formation energy signifies dynamical instability. In the case of Si_2PBi, when the formation energy slightly exceeds 0 eV and becomes positive, it indicates an unstable state for the system [59], the all systems except Si_2PBi are dynamically stable (Table 1). This was confirmed by the phonon dispersion spectrum of the Si_2XY systems, which indicates that the Si_2PBi system is less dynamically stable compared to other Si_2XY systems, as previously reported in the context of the Rashba effect [37]. The AIMD simulation provided insights into the thermal stability and dynamic behavior of the 2D material. The canonical (NVT) ensemble with Andersen thermostat was employed to obtain the results of the AIMD. To assess the thermodynamic stability of these monolayers at room temperature, a $5 \times 5 \times 1$ supercell was utilized, consistent with previous studies on 2D systems [60–63], employing a 5 ps simulation duration with a 1 fs time step. The energy convergence over time is illustrated in Fig. 2. The Si_2XY systems were all set up to operate at 300 K. Over time, the total energy of each system varied to within a small 1 eV energy range of the next after a 1 ps time interval. After the simulation, minimal alterations or negligible deformation and no sign of a bond break were observed in the structural elements of Si_2XY systems, including Si_2PBi. This analysis demonstrates the dynamical stability of all Si_2XY systems at ambient temperature. Over the 5 ps simulation period, the material maintained its structural integrity without any signs of significant degradation or phase transformation. This indicates the feasibility of conducting experiments on appropriate material substrates for synthesis.

3.2. Electronic properties

For the electronic characteristic of Si_2XY combination systems the PBE and hybrid HSE06 methods are used to determine the electronic band structure using KΓMK path that are displayed in Fig. 3. Except for Si_2PBi and Si_2AsBi, which are metallic and direct bandgap semiconductors at Γ-point (Fig. 3(e)), all the examined systems are indirect by default, respectively. The anticipated energy gap values for Si_2XY systems, as determined using the PBE method, are presented in Table 1. These values align well with previous theoretical investigations [37].

The arrangement of bonds and the resulting electronic structure contribute to the formation of energy bands. The energy gap between the valence and conduction bands arises due to differences in energy levels of the molecular orbitals formed by the Si-X, Si–Y, and Si–Si bonds. The specific arrangement of bonds and the resulting electronic structure determine the size and nature of the band gap in the Si_2XY hexagonal structures. It is intriguing to note that these binary compounds exhibit conduction band minima (CBM) at the M-point, except for Si_2PBi, where it is observed at the Γ-point, coinciding with the location of the valence band maxima (VBM). In Fig. 3(a), Si_2PAs demonstrates a higher energy band gap of 2.009 eV with the HSE06 compared to 1.291 eV using the PBE, 1.308 eV by SOC [37] and remains indirect, while in Fig. 3(c), the initially metallic Si_2PBi transitions to a semiconducting state with a 0.478 eV energy band gap by implementation of the HSE06 functional. This opening of the band gap by

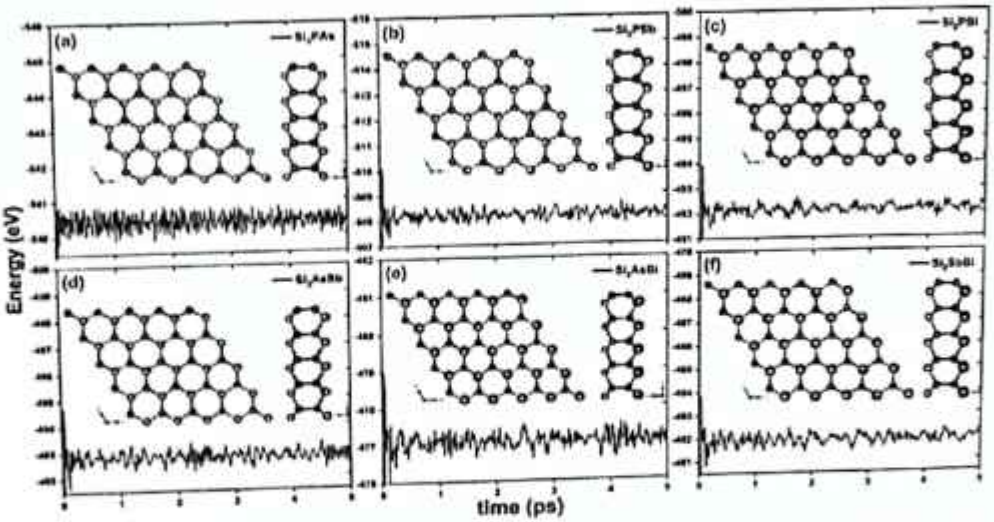

Fig. 2. (a–f) The change in energy of systems with respect to time(ps) of Si_2XY with final snap shot of stucture at ambient temperature.

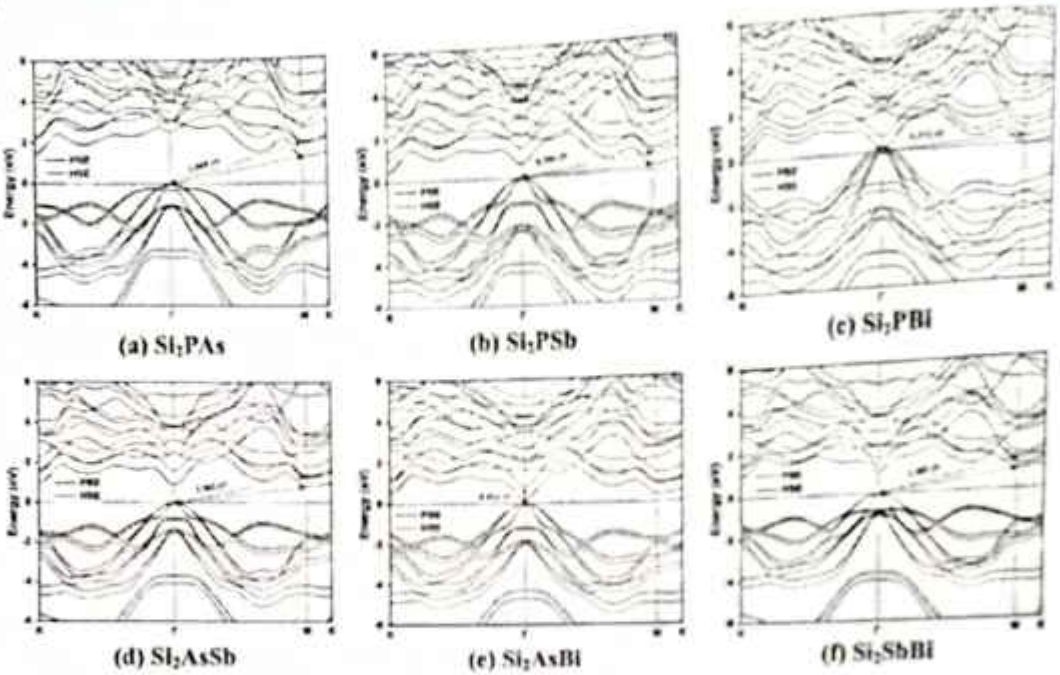

Fig. 3. Using the PBE and HSE06 technique, the electronic band structure of Si_2XY systems (It is zero to establish the Fermi level).

hybrid HSE06 is a range-separated hybrid functional that combines semilocal exchange with a fraction of Fock exchange [34]. Furthermore, Fig. 3(e) illustrates that Si_2AsBi maintains a direct band gap nature at the Γ-point with an energy gap of 0.816 eV, and an increase in band gap values is observed in the remaining systems with the transition from the PBE to the HSE06 functional.

We conducted a detailed examination of the projected density of states (PDOS) to explore various orbital contributions and elucidate the electronic structures of Si_2XY-based systems employing the PBE method. As depicted in Fig. 4, the electron density of p-orbitals originating from Si, X, and Y elements predominates in both the conduction and valence band regions, with limited involvement of the s-orbital from group-V elements. Notably, hybridization between the Si *s* and *p* orbitals and the *p*-orbitals of group-V elements is observed, contributing to the electronic structure. Specifically, in the Si_2PAs system (Fig. 4(a)), overlapping of Si-3p, P-3p, and As-4p orbitals near the Fermi level results in band gap opening. Similarly, for Si_2PSb (Fig. 4(b)), overlapping of Si-3p and Sb-5p orbitals near the Fermi level in the valence band leads to the formation of a small band gap. Conversely, Si_2PBi exhibits metallic behavior (Fig. 4(c)) due to the occupancy of Si, P, and Bi element orbital electrons at the Fermi level. In Si_2AsSb, the overlapping of Si-3p and Sb-5p orbitals contributes to a small band gap, while in Si_2SbBi, the absence of valence electrons in Sb-5p or Bi-6p orbitals results in unoccupied states at the Fermi level, leading to its semiconductor nature (Fig. 4(f).

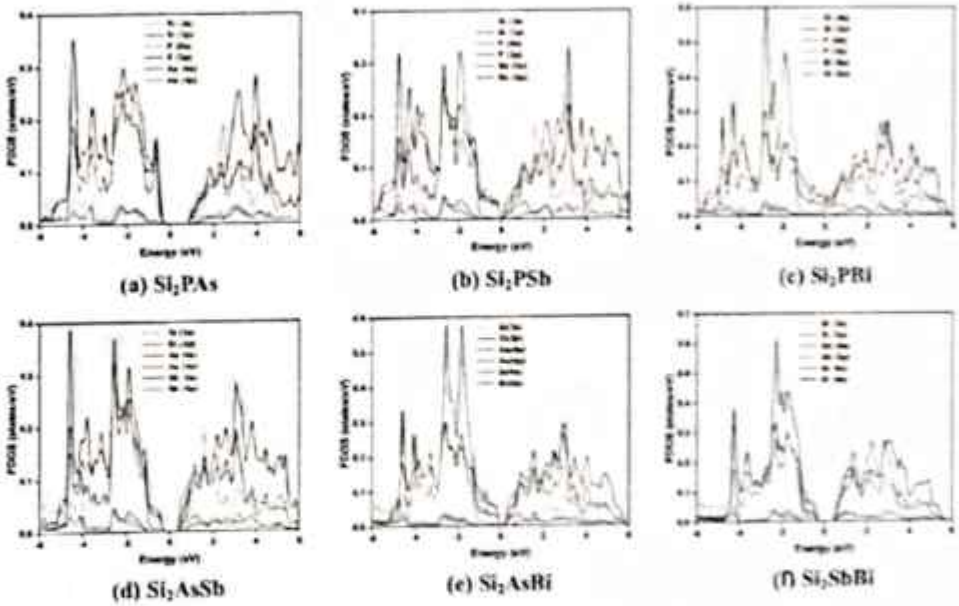

Fig. 4. The projected density of states of electron for all respective Si_2XY system (a–f).

e)). The overlap's strong hybridization indicates at the formation of covalent bonds. Additionally, Si-3*p* orbitals play a significant part in the formation of Si_2PAs valence band, whereas Si-3*p* orbitals play an essential part in the generation of the conduction band, along with P-3*p*, As-4*p*, and Si-3*s* orbitals. This exemplifies the process of orbital hybridization. The electrostatic profile is defined by the work function of a system, denoted by φ, is defined as $\varphi = V - EF$ [65], here, V denotes the electrostatic potential in the vacuum near the surface, and E_F signifies the Fermi level within the material. The work function represents the minimum energy needed for an electron to transition from the Fermi level to the vacuum level, elucidating its capability to escape the material surface. The calculated work function and potential difference (ΔV) values for each respective Si_2XY system are shown in Fig. 5, with a vacuum level and Fermi-level indication and value (Table 1). From the Figure, it is evident that the ΔV arises due to the dipole moment along the asymmetry in the Z direction between the upper and bottom surfaces in Janus Si_2XY [66]. This phenomenon is described by the Helmholtz model [67], where the dipole moment is linearly proportional to ΔV, which was noticed in BiXY Janus systems [68]. Additionally, ΔV increases with the atomic size of X relative to Y, or vice versa. Specifically, in the Si_2PAs to Si_2PSb systems, ΔV increases from 0.269 eV to 0.559 eV, respectively. A similar trend is observed in other Si_2XY systems. In this context, it is observed that certain systems exhibit a minor potential difference, which may arise as a result of the positive charge distribution along the boundary of X and Y atoms within the Si_2XY system [69–71]. The Si_2PAs have a higher band gap than other Si_2XY systems; the electron requires more energy to transition from Fermi-level to vacuum-level (Fig. 5(a)).

3.3. *Strain engineering*

To evaluate the durability of the electrical bandgap and to investigate the effects of tensile and compressive strain, we applied biaxial strain to the Si_2XY systems. Manipulating the electronic properties of nanomaterials by strain engineering is regarded as a useful method.

To explore the deformation effects, the biaxial strain is applied to the hexagonal Si_2XY systems up to about 10 % with change of ± 2 % by altering the lattice constant. We observed a transition in the electronic band energy gap upon the application of biaxial strain, as depicted in Fig. 6. The impact of isotropic biaxial strains is expressed as $\varepsilon = (a - a_0)/a_0$[73], where a_0 and a are the respective lattice parameters for the unstrained and strained instances. Here, in all hexagonal lattice systems (a = b), the strain is introduced by adjusting the lattice parameters within a range of approximately 2 %. We inspected the strain energy per unit atom using the equation, $E_s = (E_{strained} - E_{unstrained})/n$ in order to validate that the employed biaxial strains are in the elastic domain, where n denotes how many atoms make up a unit cell. Fig. 6(a) illustrates a strain range of approximately ±10 % across all systems, which remains within the elastic limit as indicated by the strain energy curve. The curve exhibits a quadratic trend, suggestive of reversible behavior. The Si_2PAs offers more of an energy difference than Si_2PSb, Si_2PBi, Si_2AsSb, Si_2AsBi, and Si_2SbBi systems. The non-monotonic tendency occurs by the high electro-negative N atoms as compared with P, As, Sb, and Bi. Comparing Si_2PAs to other systems under strain, Si_2AsBi exhibits lower energy band gap values, whereas Si_2PAs exhibit higher energy bandgap values of 1.377 eV. Fig. 6(b) depicts the alteration of the bandgap under varied applied biaxial strains. This might spark interest in using it in flexible electronic devices in the future.

With the exception of Si_2PBi, all systems that are indirect bandgap semiconductors maintain their indirect character during tensile strain, the VBM at Γ-point and the CBM at M-point. Furthermore, the compressive strain preserves its inadvertent form, and CBM does not change for all systems from the M to K point. At strain levels of 4 % and 6 % for Si_2PSb, the material exhibits a transition to a direct bandgap semiconductor with energy band gap values of 0.487 eV and 0.499 eV near the Γ-point, respectively, while at 8 % strain, it reverts to an indirect bandgap semiconductor with an energy band gap value of 0.386 eV under tensile strain (Fig. 11). Similarly, for Si_2AsSb, the material undergoes a transition to direct bandgap behavior at 2 % and 4 % strain, with energy band gap values of 0.755 eV and 0.664 eV near the Γ-point, respectively, and at 6 % strain, it reverts to an indirect bandgap semiconductor with an energy band gap value of 0.441 eV (Fig. 7). Conversely, all systems exhibit indirect bandgap semiconductor behavior under compressive strain. Si_2PBi exhibits a transition from metallic to semiconducting behavior within the strain range of 2 %–8 %, with a direct bandgap of 0.246 eV observed at 10 % strain near the Γ-point (Fig. 8). Si_2SbBi demonstrates direct bandgap behavior with energy band gap values of 0.822 eV and 0.656 eV at 2 % and 4 % strain, respectively (Fig. 12). Si_2AsBi exhibits direct bandgap behavior at 2 % strain with an energy band gap value of 0.074 eV, transitioning to

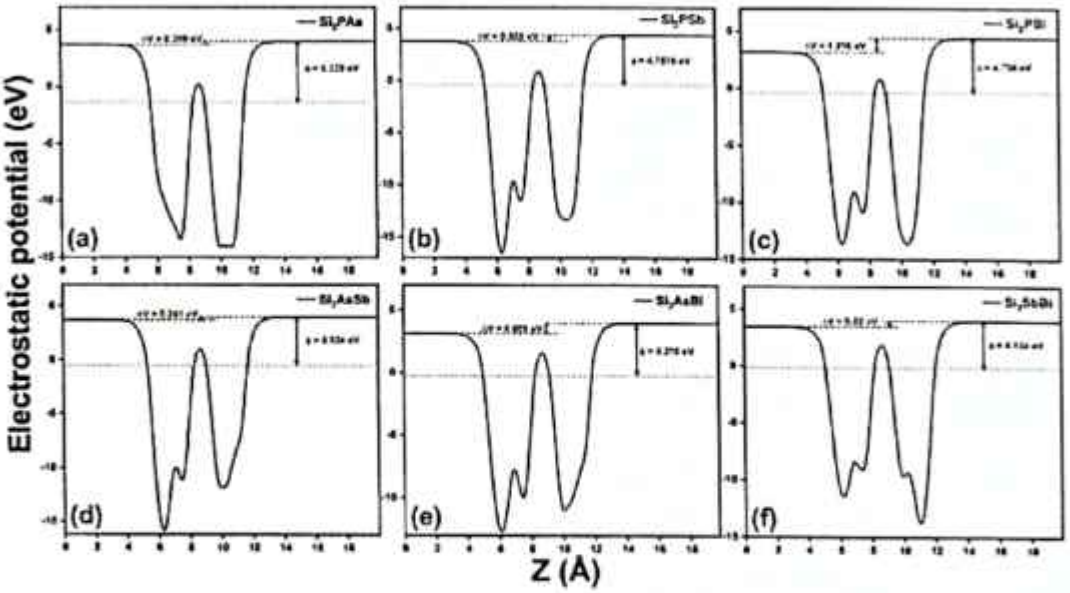

Fig. 5. The electrostatic profile of Si_2XY systems (a–f), respectively.

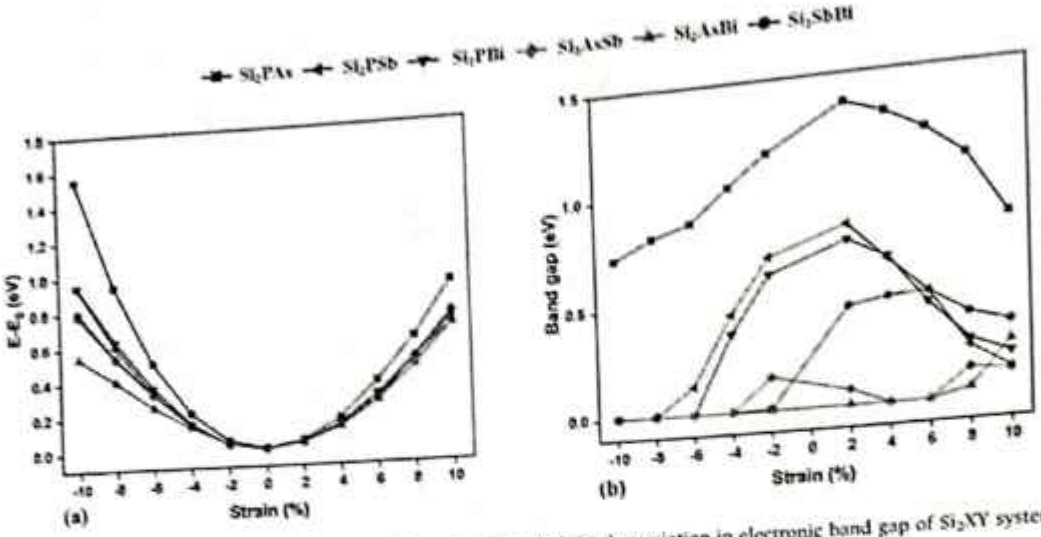

Fig. 6. By employing biaxial strain, (a) a variation in energy curve and (b) the variation in electronic band gap of Si_2XY systems.

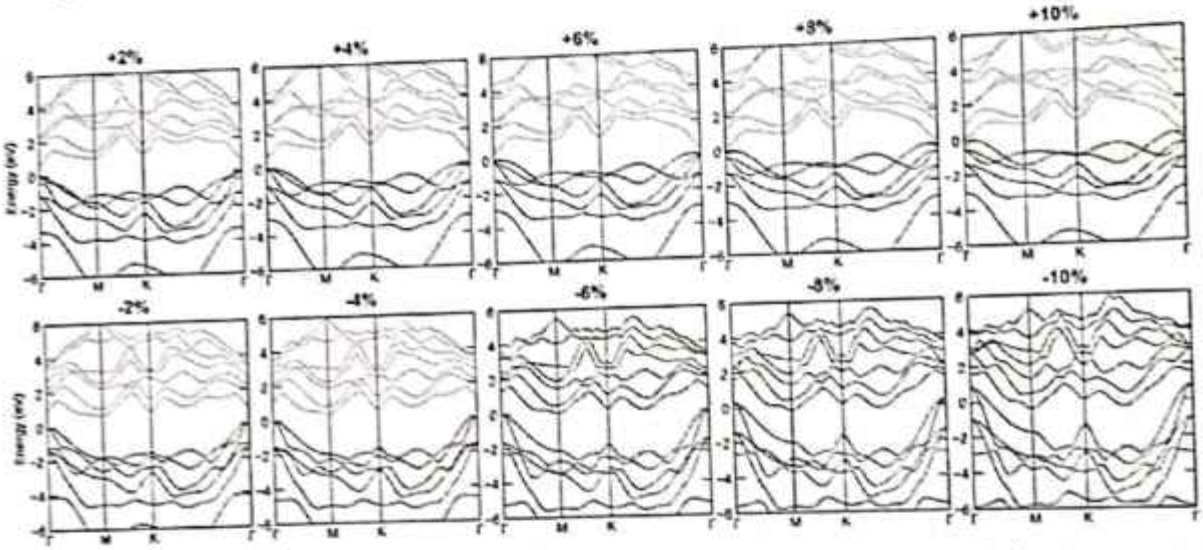

Fig. 7. The electronic band structures of Si_2AsSb with using strain from ± 2 % to ± 10 %, respectively.

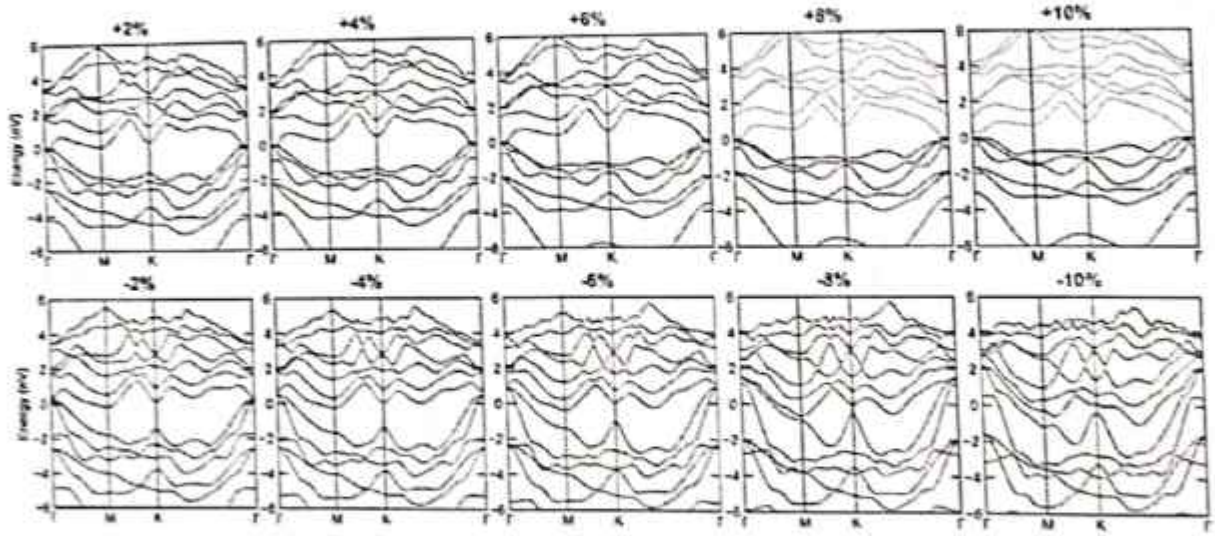

Fig. 8. The electronic band structures of Si_2PBi with using strain from ± 2 % to ± 10 %, respectively.

metallic behavior at 4 % and 6 % strain, and reverting to semiconducting behavior at 8 % and 10 % strain with indirect bandgap values of 0.132 eV and 0.119 eV, respectively (Fig. 9).The Si_2PAs become indirect under compressive strain but remain direct band gaps at tensile strain (Fig. 10). From these strain engineering characteristics, we can customize the energy of the material as well as the electronic mechanism or semiconducting nature in terms of the energy band gap of Si_2XY-based systems.

3.4. Optical properties

Additionally, we looked into the Si_2XY systems's optical properties. When examining the characteristics and potential uses of novel 2D materials, the dielectric function is essential. The optical characteristics of the system are characterized by its frequency-dependent complex dielectric function. DFT with independent particle approximation (IPA) was used to determine the dielectric function's real and imaginary components, absorption spectra, refractive index, reflectivity, and electron energy loss spectroscopy (EELS) for the materials Si_2PAs, Si_2PSb, Si_2PBi, Si2AsBi, Si_2AsBi, and Si_2SbBi [72,73]. The dielectric function is referred to as the linear response of any material to electromagnetic radiations and is denoted by the formula,

$$\varepsilon(\omega) = \varepsilon_r(\omega) + i\varepsilon_i(\omega) \tag{3}$$

Here, the complex dielectric function's real and imaginary parts are denoted by $\varepsilon_r(\omega)$ and $\varepsilon_i(\omega)$, respectively (Eq. 3). It is possible to determine the imaginary part by adding up the electronic states. The Kramers-Kroning relationship indicates that there is a significant relationship between the real and imaginary part [74–76]. Fig. 13(a), the optical spectrum is conducted in the (E ||X) plane to enhance the effects, as the 2D material possesses a large surface area-to-volume ratio. The real component of $\varepsilon r(\omega)$ provides the static dielectric constant value at zero energy. The static dielectric constants for Si_2PAs, Si_2PSb, Si_2PBi, Si_2AsSb, Si_2AsBi, and Si_2SbBi systems along the (E ||X) direction are 5.213, 6.197, 13.987, 6.192, 8.053, and 7.517, respectively. In the (E || X) direction, negative values observed in the real component of all systems indicate their metallic behavior within the energy range of 2–5 eV, ranging from −0.7 to −3.2. The real part values stabilize uniformly beyond 15 eV. The plot of the imaginary component exhibits numerous spikes attributed to interband transitions between the VBM and CBM. The prominent spikes observed along the (E ||X) direction for the Si_2PAs, Si_2PSb, Si_2PBi, Si_2AsSb, Si_2AsBi, and Si_2SbBi systems are as follows: 24.10, 17.451, 16.125, 20.434, 18.811, and 22.914, respectively, occurring within the photon energy range of 2.5–4 eV (Fig. 13(b)). The reflectivity R(ω) and energy loss spectra of electron L(ω) evaluation expressions are presented as,

$$R(\omega) = \frac{|n(\omega)-1|^2 + k^2(\omega)}{|n(\omega)+1|^2 + k^2(\omega)} \tag{4}$$

$$L(\omega) = \frac{\varepsilon_i(\omega)}{\varepsilon_r(\omega)^2 + \varepsilon_i(\omega)^2} \tag{5}$$

Fig. 15, It is probable to determine how incident light responds with a material as it passes through it by using the frequency-dependent dielectric function. In light of this, the light absorption coefficient is most appropriately described as [31]:

$$\alpha(\omega) = \frac{\sqrt{2}\omega}{c}\left[\sqrt{\varepsilon_r^2(\omega) + \varepsilon_i^2(\omega)} - \varepsilon_r(\omega)\right]^{1/2} \tag{6}$$

The figure clearly illustrates the dependence of the dielectric function on the polarization direction of light across the six systems. A higher dielectric constant value reflects greater polarizability within the systems. In the real component of the dielectric function, the zero-frequency limit, particularly significant, represents the electronic contribution to the static dielectric constant. This real component is inversely proportional to the bandgap (E_g) and is expressed as $\varepsilon_r(0) \approx 1 + \left(\frac{\hbar\omega_p}{E_g}\right)^2$.

Fig. 13(a), which shows that the dielectric constant is high, suggests that the Si_2XY systems is highly polarizable. The electromagnetic spectrum's negative portions show a metallic pattern close to the ultraviolet region. In Fig. 13(b), there are several peaks, which emerge from the electronic transition between the conduction and valence bands.

At 0 eV photon energy, the refractive index of Si_2XY systems ranges from 2.281 to 3.722. Notably, Si_2PAs and Si_2SbBi exhibit higher refractive indices of 4.110 and 4.127, respectively, within energy ranges of 3.27 eV and 2.5 eV, as depicted in Fig. 14(a). The refractive index decreases in UV range for all systems. For Si_2PAs systems, the maximum reflectivity for both the direction of electric field of 55 % occurs at 3.97 eV seen from Fig. 14(b) (Eq 4).

The initial absorption starts from the material's respective energy band gap; for the Si_2PBi system, there is no band gap (Fig. 3(c)) by the PBE method; similarly, the optical absorption spectra of Si_2PBi start from 0 eV photon energy (Fig. 15(a)), while in other systems, the absorption starts from their respective band gaps (Eq 6). In Fig. 15(a), the initial absorption commences at the first peak of 1×10^5 cm^{-1} at 0.6 eV energy within the infrared (IR) range. Notably, a high absorption

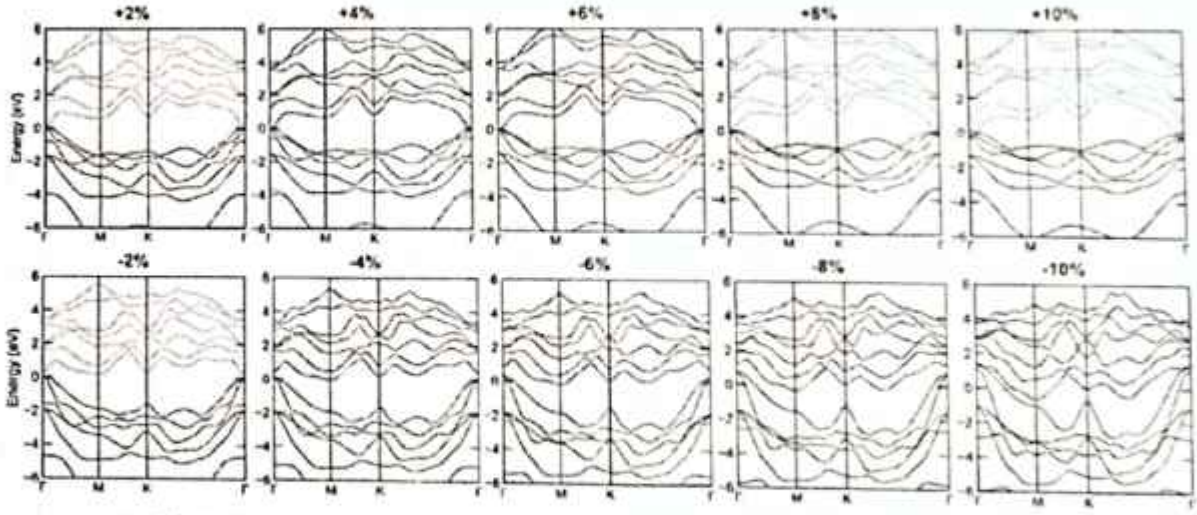

Fig. 9. The electronic band structures of Si_2AsBi with using strain from ± 2 % to ± 10 %, respectively.

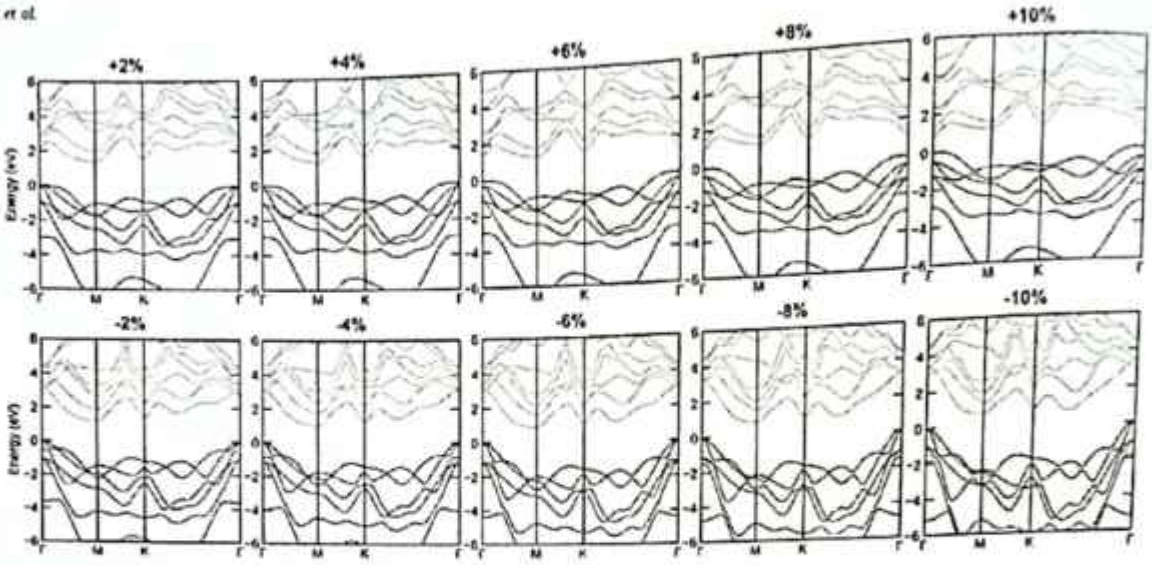

Fig. 10. The electronic band structures of Si_2PAs with using strain from ± 2 % to ± 10 %, respectively.

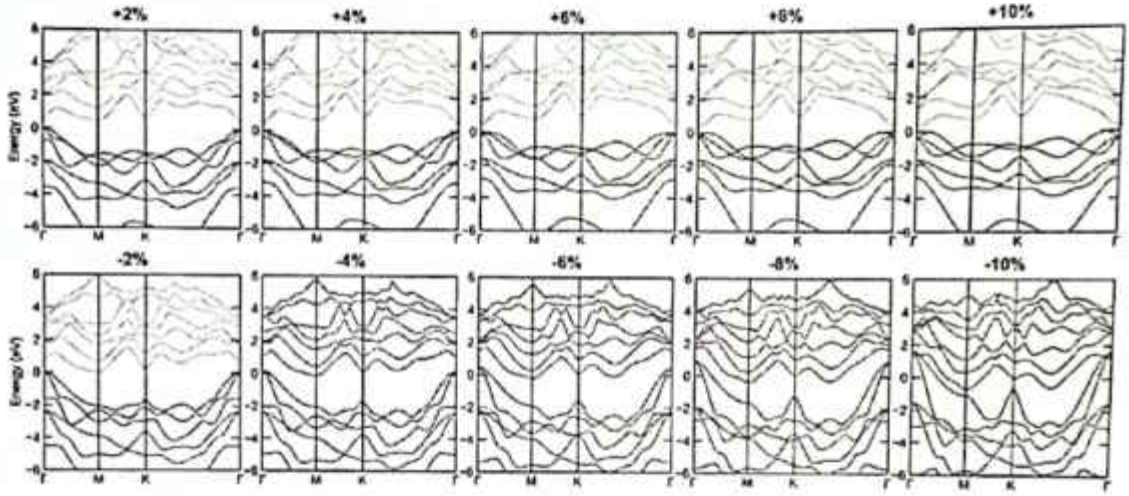

Fig. 11. The electronic band structures of Si_2PSb with using strain from ± 2 % to ± 10 %, respectively.

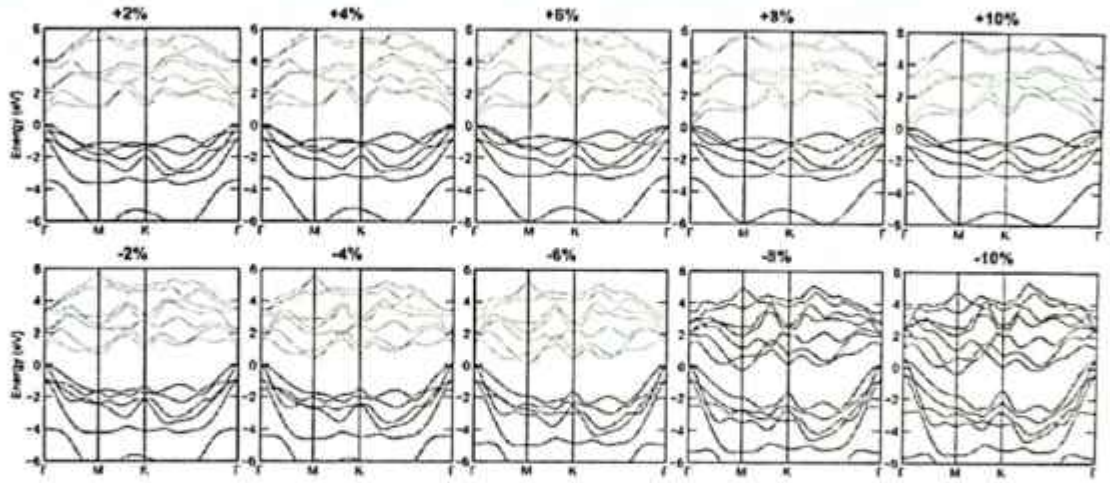

Fig. 12. The electronic band structures of Si_2SbBi with using strain from ± 2 % to ± 10 %, respectively.

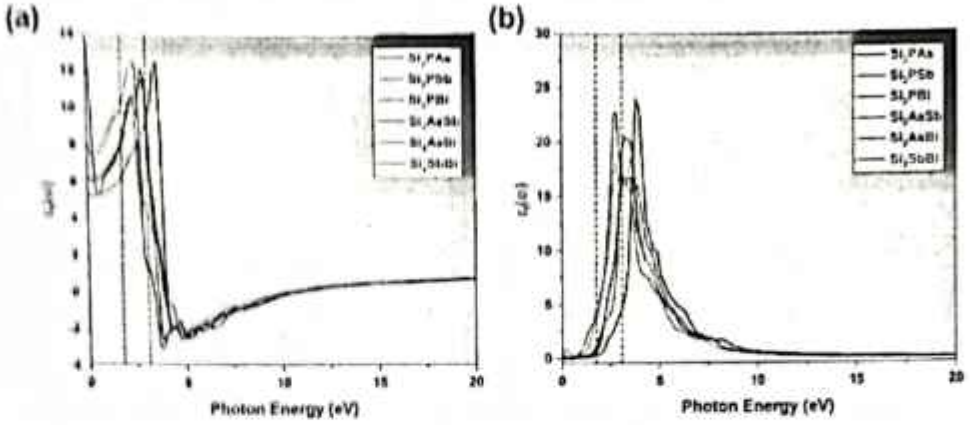

Fig. 13. (a, b) The complex dielectric function of Si_2XY systems of real and imaginary component, respectively.

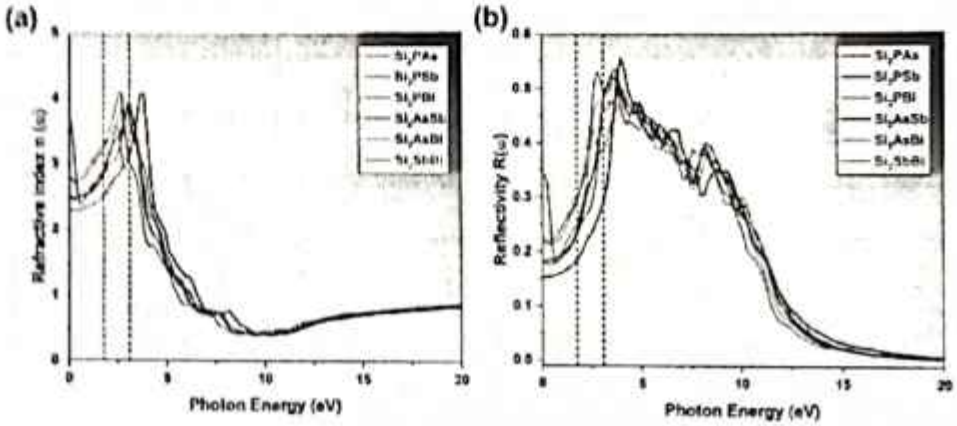

Fig. 14. (a) Refractive index (b) Reflectivity of Si_2XY systems.

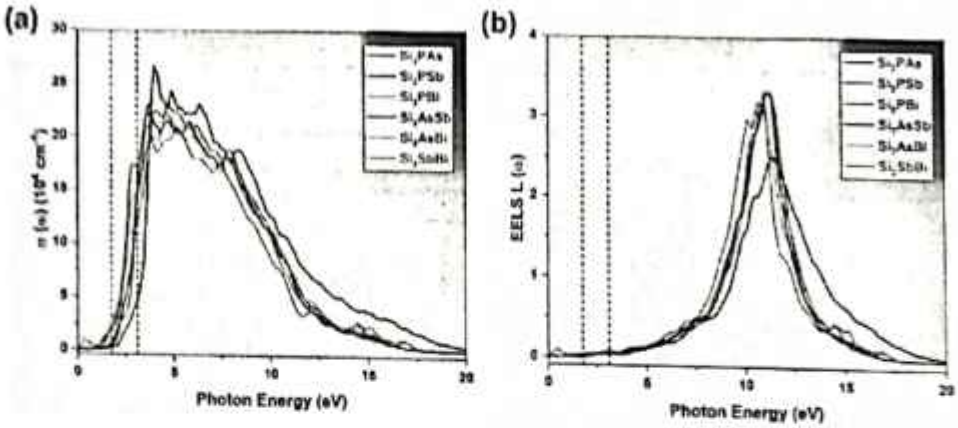

Fig. 15. (a) Absorption coefficient as the function of photon energy (b) EELS of Si_2XY systems.

coefficient of 2.65 × 10^5 cm^{-1} is observed in the UV range at 4.2 eV photon energy for the Si_2PAs system but is less than 5 eV photon energy; if absorption is greater than 5 eV, it will give better UV absorption. In Fig. 15(b), we present the electron energy loss function spectra (EELS) (Eq 5), elucidating the mechanism of energy loss in electrons as they traverse the substance, with the peaks in the loss spectrum indicative of characteristics associated with the plasma frequency. It illustrates the point of maximum resonant energy loss, occurring at 11.08 eV for the Si_2AsBi system. In the IR, visible, and UV regions, the plot displays small peaks.

4. Conclusions

The dynamical stability of Si_2XY (X, Y=P, As, Sb, Bi) systems was estimated, and we found that these compounds are stable. The existence of an indirect bandgap in these materials is shown by the locations of the

CBM at the M-point and the VBM at the Γ-point. From the band structures, the nature of the Si_2PAs, Si_2PSb, Si_2AsSb, Si_2AsBi, and Si_2SbBi (indirect bandgap) are semiconductors as well. Metallic Si_2PBi (via PBE) is semiconducting via band gap expansion utilizing the HSE06 hybrid functional. From the strain engineering of Si_2XY-based systems, we can modify electronic properties in terms of changing the energy band gap. The optical properties indicate good absorption in the UV range. The value of the absorption coefficient is in the range of $10^4 cm^{-1}$. Here, the IR, visible, and UV zones exhibit the least absorption, while high absorption coefficient of 2.65×10^5 cm^{-1} with 4.2 eV photon energy is obtained for Si_2PAs system in the UV region. This indicates that it is useful in electronic device applications. This research will help us clarify the electrical and optical properties of the systems under investigation, as well as potential applications in electronics.

CRediT authorship contribution statement

Priyankaben N. Thorat: Writing – review & editing, Writing – original draft, Validation, Methodology, Formal analysis, Conceptualization. **Aparnakumari M. Patel:** Writing – original draft, Visualization, Methodology, Investigation. **Rahulkumar P. Jadav:** Writing – review & editing, Writing – original draft, Visualization, Validation. **Radha N Somaiya:** Writing – review & editing, Writing – original draft, Validation, Supervision, Methodology, Investigation, Formal analysis, Data curation, Conceptualization. **Yogesh Sonvane:** Writing – review & editing, Visualization, Validation, Supervision, Software, Resources, Project administration, Methodology, Investigation, Funding acquisition, Formal analysis, Data curation, Conceptualization.

Declaration of competing interest

We believe that the paper may be of particular interest to the readers of your journal. The authors claim that none of the material in the paper has been published or is under consideration for publication elsewhere. The authors declare no competing financial interests.

Data availability

Data will be made available on request.

Acknowledgments

Authors are thankful to the CDAC, Param Siddhi-AI, Pune for providing computational facilities and YS is thankful to the Science and Engineering Research Board (SERB), India for the financial support (grant number: EEQ/2022/000584).

References

[1] K.S. Novoselov, A.K. Geim, S.V. Morozov, D. Jiang, Y. Zhang, S.V. Dubonos, I.V. Grigorieva, A.A. Firsov, Electric field effect in atomically thin carbon films, Science 306 (2004) 666–669, [illegible].

[2] D. Wei, F. Wang, Graphene: a partially ordered non-periodic solid, J. Chem. Phys. 141 (2014) 144701, [illegible].

[3] G.W. Flynn, Perspective: the dawning of the age of graphene, J. Chem. Phys. 135 (2011), [illegible].

[4] P. Vogt, P. De Padova, C. Quaresima, J. Avila, E. Frantzeskakis, M.C. Asensio, A. Resta, B. Ealet, G. Le Lay, Silicene: compelling experimental evidence for graphenelike two-dimensional silicon, Phys. Rev. Lett. 108 (2012) 155501, [illegible].

[5] A. Fleurence, R. Friedlein, T. Ozaki, H. Kawai, Y. Wang, Y. Yamada-Takamura, Experimental evidence for epitaxial silicene on diboride thin films, Phys. Rev. Lett. 108 (2012) 245501, [illegible].

[6] D. Jose, A. Datta, Structures and chemical properties of silicene: unlike graphene, Acc. Chem. Res. 47 (2014) 593–602, [illegible].

[7] L. Li, Y. Yu, G.J. Ye, Q. Ge, X. Ou, H. Wu, D. Feng, X.H. Chen, Y. Zhang, Black phosphorus field-effect transistors, Nat. Nanotechnol. 9 (2014) 372–377, [illegible].

[8] J. Dai, X.C. Zeng, Structure and stability of two dimensional phosphorene with =O or =NH functionalization, RSC Adv. 4 (2014) 48017–48021, [illegible].

[9] C. Jin, F. Lin, K. Suenaga, S. Iijima, Fabrication of a freestanding boron nitride single layer and its defect assignments, Phys. Rev. Lett. 102 (2009) 195505, [illegible].

[10] C. Lee, Q. Li, W. Kalb, X.Z. Liu, H. Berger, R.W. Carpick, J. Hone, Frictional characteristics of atomically thin sheets, Science 328 (2010) 76–80, [illegible].

[11] W. Lei, D. Portehault, D. Liu, S. Qin, Y. Chen, Porous boron nitride nanosheets for effective water cleaning, Nat. Commun. 4 (1 4) (2013) 1–7, [illegible].

[12] G. Wang, R. Pandey, S.P. Karna, Atomically thin group v elemental films: theoretical investigations of antimonene allotropes, ACS Appl. Mater. Interfaces 7 (2015) 11490–11496, [illegible].

[13] D. Singh, S.K. Gupta, Y. Sonvane, I. Lukačević, Antimonene: a monolayer material for ultraviolet optical nanodevices, J Mater Chem C Mater 4 (2016) 6386–6390, [illegible].

[14] Q.H. Wang, K. Kalantar-Zadeh, A. Kis, J.N. Coleman, M.S. Strano, Electronics and optoelectronics of two-dimensional transition metal dichalcogenides, Nat Nanotechnol. 7 (2012) 699–712, [illegible].

[15] S. Sahoo, A.P.S. Gaur, M. Ahmadi, M.J.-F. Guinel, R.S. Katiyar, Temperature-dependent Raman studies and thermal conductivity of few-layer MoS2, J. Phys. Chem. C 117 (2013) 9042–9047, [illegible].

[16] Y. Jeong, J. Hoon Park, J. Ahn, H. Tamura, M. Minagawa, A. Baba, M. Hiraiwa, T. Thi Nguyen, S.-I. Kuroki, R. Liu, Y. Chai, Z. Liu, Investigation of chemical vapour deposition MoS2 field effect transistors on SiO2 and ZrO2 substrates, Nanotechnology 28 (2017) 164004, [illegible].

[17] F. Wang, Z. Wang, Q. Wang, F. Wang, L. Yin, K. Xu, Y. Huang, J. He, Synthesis, properties and applications of 2D non-graphene materials, Nanotechnology 26 (2015), [illegible].

[18] K. Onyebuchi Okeke, C.N.M. Ouma, G. Gebreyesus, P. Hess, Relationships between the elastic and fracture properties of borophene and molybdenum disulfide and those of graphene, Nanotechnology 28 (2017) 064002, [illegible].

[19] D. Singh, S.K. Gupta, Y. Sonvane, A. Kumar, R. Ahuja, 2D-HfS2 as an efficient photocatalyst for water splitting, Catal. Sci. Technol. 6 (2016) 6605–6614, [illegible].

[20] D. Singh, S.K. Gupta, Y. Sonvane, S. Sahoo, Modulating the electronic and optical properties of monolayer arsenene phases by organic molecular doping, Nanotechnology 28 (2017), [illegible].

[21] C. Barreteau, B. Michon, C. Besnard, E. Giannini, High-pressure melt growth and transport properties of SiP, SiAs, GeP, and GeAs 2D layered semiconductors, J. Cryst. Growth 443 (2016) 75–80, [illegible].

[22] W. He, W. Ruan, Y. Yang, W. Shi, Y. Xu, H. Sepehrian, G. Djogo, J. Li, S. Hu, S. Zhang, S. Guo, Y. Huang, Z. Zhu, B. Cai, M. Xie, W. Zhou, H. Zeng, Two-dimensional SiP: an unexplored direct band-gap semiconductor, 2D Mater. 4 (2016) 015030, [illegible].

[23] P. Zhao, J. Li, W. Wei, Q. Sun, H. Jin, B. Huang, Y. Dai, Giant anisotropic photogalvanic effect in a flexible AsSb monolayer with ultrahigh carrier mobility, Phys. Chem. Chem. Phys. 19 (2017) 27233–27239, [illegible].

[24] W. Zhang, J. Yin, Y. Ding, Y. Jiang, P. Zhang, Strain-engineering tunable electron mobility of monolayer IV–V group compounds, Nanoscale 10 (2018) 16750–16758, [illegible].

[25] B. Huang, H.L. Zhuang, M. Yoon, B.G. Sumpter, S.H. Wei, Highly stable two-dimensional silicon phosphides: different stoichiometries and exotic electronic properties, Phys Rev B Condens Matter Mater Phys 91 (2015) 121401, [illegible].

[26] M. Ashton, S.B. Sinnott, R.G. Hennig, Computational discovery and characterization of polymorphic two-dimensional IV–V materials, Appl. Phys. Lett. 109 (2016) 192103, [illegible].

[27] B. Ozdamar, G. Ozbal, M.N. Çinar, K. Sevim, G. Kurt, B. Kaya, H. Sevinçli, Structural, vibrational, and electronic properties of single-layer hexagonal crystals of group IV and V elements, Phys. Rev. B 98 (2018) 045431, [illegible].

[28] A. Bafekry, F. Shojai, D.M. Hoat, M. Shahrokhi, M. Ghergherehchi, C. Nguyen, The mechanical, electronic, optical and thermoelectric properties of two-dimensional honeycomb-like of XSb (X = Si, Ge, Sn) monolayers: a first-principles calculations, RSC Adv. 10 (2020) 30398–30405, [illegible].

[29] P. Zhao, Y. Liang, Y. Ma, B. Huang, Y. Dai, Janus chromium dichalcogenide monolayers with low carrier recombination for photocatalytic overall water-splitting under infrared light, J. Phys. Chem. C 123 (2019) 4186–4192, [illegible].

[30] J. Zhang, S. Jia, I. Kholmanov, L. Dong, D. Er, W. Chen, H. Guo, Z. Jin, V.B. Shenoy, L. Shi, J. Lou, Janus monolayer transition-metal dichalcogenides, ACS Nano 11 (2017) 8192–8198, [illegible].

[31] A.Y. Lu, H. Zhu, J. Xiao, C.P. Chuu, Y. Han, M.H. Chiu, C.C. Cheng, C.W. Yang, K.H. Wei, Y. Yang, Y. Wang, D. Sokaras, D. Nordlund, P. Yang, D.A. Muller, M.Y. Chou, X. Zhang, L.J. Li, Janus monolayers of transition metal dichalcogenides, Nat. Nanotechnol. 12 (2017) 744–749, [illegible].

[32] J. Wang, H. Shu, T. Zhao, P. Liang, N. Wang, D. Cao, X. Chen, Intriguing electronic and optical properties of two-dimensional Janus transition metal dichalcogenides, Phys. Chem. Chem. Phys. 20 (2018) 18571–18578, [illegible]

[33] W. Zhou, J. Chen, Z. Yang, J. Liu, F. Ouyang, Geometry and electronic structure of monolayer, bilayer, and multilayer Janus WSSe, Phys. Rev. B 99 (2019) 075160, [illegible]

[34] C. Barreteau, B. Michon, C. Besnard, E. Giannini, High-pressure melt growth and transport properties of SiP, SiAs, GeP, and GeAs 2D layered semiconductors, J. Cryst. Growth 443 (2016) 75–80, [illegible]

[35] W. He, W. Bian, Y. Yang, W. Shi, Y. Xu, H. Sepehrian, G. Dyngo, J. Li, S. Hu, S. Zhang, S. Guo, Y. Huang, Z. Zhu, B. Cai, M. Xie, W. Zhou, H. Zeng, Two-dimensional SiP, an unexplored direct band gap semiconductor, 2D Mater. 4 (2016) 015030, [illegible]

[36] P. Zhao, J. Li, W. Wei, Q. Sun, H. Jin, B. Huang, Y. Dai, Giant anisotropic photogalvanic effect in a flexible AsSb monolayer with ultrahigh carrier mobility, Phys. Chem. Chem. Phys. 19 (2017) 27233–27239, [illegible]

[37] S. Babaee Touski, N. Ghobadi, Structural, electrical, and Rashba properties of monolayer Janus Si2XY (X,Y = P, As, Sb, and Bi), Phys. Rev. B 103 (2021) 165404, [illegible]

[38] Y. Wu, C.H. Yang, H.N. Zhang, L.H. Zhu, X.Y. Wang, Y.Q. Li, S.Y. Zhu, X.C. Wang, The flexible Janus X2PAs (X = Si, Ge and Sn) monolayers with in-plane and out-of-plane piezoelectricity, Appl. Surf. Sci. 589 (2022), [illegible]

[39] A. Li, K. Zhang, X. Zeng, N. Li, J. Wang, Electronic and photochemical properties of hybrid binary silicon and germanium derived Janus monolayers, Phys. Chem. Chem. Phys. 23 (2021) 17502–17511, [illegible]

[40] T.V. Vu, V.T.T. Vi, C.V. Nguyen, H.V. Phuc, N.N. Hieu, Computational prediction of electronic and optical properties of Janus Ga 2 SeTe monolayer, J. Phys. D Appl. Phys. 53 455302 Journal of Physics D: Applied Physics J. Phys. D: Appl. Phys 53 (2020) 10, [illegible]

[41] L.C. Nhan, C.Q. Nguyen, N.V. Hieu, H.V. Phuc, C.V. Nguyen, N.N. Hieu, T.V. Vu, H.T.T. Nguyen, Theoretical insights into tunable electronic and optical properties of Janus Al2SSe monolayer through strain and electric field, Optik 238 (2021), [illegible]

[42] P.E. Blöchl, Projector augmented wave method, Phys. Rev. B 50 (1994) 17953, https://doi.org/10.1103/PhysRevB.50.17953.

[43] G. Kresse, J. Furthmüller, Efficient iterative schemes for ab initio total-energy calculations using a plane-wave basis set, Phys. Rev. B 54 (1996) 11169, https://doi.org/10.1103/PhysRevB.54.11169.

[44] G. Kresse, D. Joubert, From ultrasoft pseudopotentials to the projector augmented-wave method, Phys. Rev. B 59 (1999) 1758, https://doi.org/10.1103/PhysRevB.59.1758.

[45] G. Kresse, J. Hafner, *Ab initio* molecular dynamics for liquid metals, Phys. Rev. B 47 (1993) 558, https://doi.org/10.1103/PhysRevB.47.558.

[46] G. Kresse, D. Joubert, From ultrasoft pseudopotentials to the projector augmented-wave method, Phys. Rev. B 59 (1999) 1758, https://doi.org/10.1103/PhysRevB.59.1758.

[47] J.P. Perdew, K. Burke, M. Ernzerhof, Generalized gradient approximation made simple, Phys. Rev. Lett. 77 (1996) 3865, https://doi.org/10.1103/PhysRevLett.77.3865.

[48] N. Shuichi, Constant temperature molecular dynamics methods, Prog. Theor. Phys. Suppl. 103 (1991) 1–46, https://doi.org/10.1143/PTPS.103.1.

[49] H.C. Andersen, Molecular dynamics simulations at constant pressure and/or temperature, J. Chem. Phys. 72 (1980) 2384–2393, https://doi.org/10.1063/1.439486.

[50] K. Momma, F. Izumi, VESTA 3 for Three-Dimensional Visualization of Crystal, Volumetric and Morphology Data, vol 44, Urn:Issn, 2011, pp. 1272–1276, https://doi.org/10.1107/S0021889811038970, 0021-8898.

[51] S. Babaee Touski, N. Ghobadi, Structural, electrical, and Rashba properties of monolayer Janus Si2XY (X,Y = P, As, Sb, and Bi), Phys. Rev. B 103 (2021) 165404, [illegible]

[52] R.N. Somaiya, D. Singh, Y. Sonvane, S.K. Gupta, R. Ahuja, Potential SiX (X = N, P, As, Sb, Bi) homo-bilayers for visible-light photocatalyst applications, Catal. Sci. Technol. 11 (2021) 4996–5013, [illegible]

[53] B. Özdamar, G. Özbal, M.N. Çınar, K. Sevim, G. Kurt, B. Kaya, H. Sevinçli, Structural, vibrational, and electronic properties of single-layer hexagonal crystals of group IV and V elements, Phys. Rev. B 98 (2018) 045431, [illegible]

[54] E. Deligoz, H. Ozisik, K. Colakoglu, Theoretical predictions of the structural, mechanical and lattice dynamical properties of XW2 (X = Zr, Hf) Laves phases, Phil. Mag. 94 (2014) 1379–1392, [illegible]

[55] R.N. Somaiya, D. Singh, Y. Sonvane, S.K. Gupta, R. Ahuja, Potential SiX (X = N, P, As, Sb, Bi) homo-bilayers for visible-light photocatalyst applications, Catal. Sci. Technol. 11 (2021) 4996–5013, [illegible]

[56] P.F. Liu, T. Bo, Z. Liu, O. Eriksson, F. Wang, J. Zhao, B.T. Wang, Hexagonal M2C3 (M = As, Sb, and Bi) monolayers: new functional materials with desirable band gaps and ultrahigh carrier mobility, J. Mater. Chem. C Mater. 6 (2018) 12689–12697, [illegible]

[57] S.S. Lin, Light-emitting two-dimensional ultrathin silicon carbide, J. Phys. Chem. C 116 (2012) 3951–3955, [illegible]

[58] N. Nasadegh, M. Naseri, S. Rezaee, Visible light response in 2D QBi (Q=Si, Ge and Sn) monolayer semiconductors: a DFT based study, Mater. Today Commun. 35 (2023) 105686, [illegible]

[59] L. Zhou, Y. Guo, J. Zhao, GeAs and SiAs monolayers: novel 2D semiconductors with suitable band structures, Physica E Low Dimens Syst Nanostruct 95 (2018) 149–153, [illegible]

[60] Z. Lu, Y. Kang, Y. Du, X. Ma, W. Ma, J. Zhang, Functionalizing Janus-structured Ti2B2 unveils exceptional capacity and performance in lithium-ion battery anodes, J. Colloid Interface Sci. 661 (2024) 662–670, [illegible]

[61] S.J. Huang, T. Zhang, Z.Y. Zeng, H.Y. Geng, X.R. Chen, Density functional theory prediction of thermoelectric properties of two-dimensional Janus HfXY (X = Te, S; Y = Cl, Br, I) monolayers with high carrier mobilities, Vacuum 224 (2024) 113142, [illegible]

[62] Y. Zhao, B. Zhang, J. Lin, Metal-free Janus α- and β-SiCP 4 : designing stable and efficient two-dimensional semiconductors for water splitting, Phys. Chem. Chem. Phys. 25 (2023) 26666–26678, [illegible]

[63] T. Iqbal, G. Rehman, Saifullah, I. Khan, R. Ahmad, I. Ahmad, Optical and photocatalytic studies of the novel 2D penta-M4P4X2Y2 (M = Pd, Pt; X≠Y: S, Se, Te) Janus monolayers, Mater. Sci. Semicond. Process. 173 (2024) 108131, [illegible]

[64] J. Yang, S. Falletta, A. Pasquarello, Range-separated hybrid functionals for accurate prediction of band gaps of extended systems, npj Comput. Mater. 9 (1–9) (2023) 1–9, [illegible]

[65] G. Hu, V. Fung, J. Huang, P. Ganesh, Work function engineering of 2D materials: the role of polar edge reconstructions, J. Phys. Chem. Lett. 12 (2021) 2320–2326, [illegible]

[66] R.N. Somaiya, A. Alam, Quasi-2D PdSe2-xGexS4 (x = 0, 1, 2): promising candidates for spontaneous overall water splitting, ACS Appl. Energy Mater. 6 (2023) 7578–7586, [illegible]

[67] Robert Dautray, J. Louis Lions, Mathematical analysis and numerical methods for science and Technology : volume 5 evolution problems I, 742, [illegible], 2000. (Accessed 13 May 2024).

[68] M.J. Varjovi, E. Durgun, First-principles study on structural, vibrational, elastic, piezoelectric, and electronic properties of the Janus BiXY (X = S, Se, Te and Y = F, Cl, Br, I) monolayers, Phys. Rev. Mater. 5 (2021) 104001, [illegible]

[69] R.M. Meftakhutdinov, R.T. Sibatov, Janus type monolayers of S-MoSiN2 family and van der waals heterostructures with graphene: DFT-based study, Nanomaterials 12 (2022), [illegible]

[70] X. Wang, S. Zhang, Y. Wang, S. Yu, B. Huang, Y. Dai, W. Wei, Structural engineering brings new electronic properties to Janus ZrSSe and HfSSe monolayers, Phys. Chem. Chem. Phys. 24 (2022), [illegible]

[71] M.J. Varjovi, S. Ershadrad, B. Sanyal, Structural, vibrational, elastic, electronic, and piezoelectric properties of binary γ-GeX and ternary γ-Ge2XX′ monolayers (X, X′ = S, Se, and Te), Phys. Rev. B 107 (2023), [illegible]

[72] S.L. Adler, Quantum theory of the dielectric constant in real solids, Phys. Rev. 126 (1962) 413, [illegible]

[73] N. Wiser, Dielectric constant with local field effects included, Phys. Rev. 129 (1963) 62, [illegible]

[74] R.N. Somaiya, Y. Sonvane, S.K. Gupta, Exploring the transport and optoelectronic properties of silicon diselenide monolayer, Superlattices Microstruct. 150 (2021), [illegible]

[75] R.N. Somaiya, Y. Sonvane, S.K. Gupta, Van der waals SiSe2 homo-bilayers for optoelectronics applications, Superlattices Microstruct. 152 (2021), [illegible]

[76] A. Marjaoui, M. Ait Tamerd, M. Zanouni, M. Diani, Strain enhanced electronic and optical properties in Janus monolayers AsMX2 (M: Sb, Bi), Physica B Condens Matter 642 (2022), [illegible]